Applied Catalysis B: Environmental 111–112 (2012) 614–620

Contents lists available at SciVerse ScienceDirect

Applied Catalysis B: Environmental

journal homepage: www.elsevier.com/locate/apcatb

Iron-catalyzed nitrogen removal as N_2 from PAN-derived activated carbon

Yasuhiro Ohshima [a], Naoto Tsubouchi [b,*], Yasuo Ohtsuka [a]

[a] Institute of Multidisciplinary Research for Advanced Materials, Tohoku University, Sendai 980-8577, Japan
[b] Center for Advanced Research of Energy and Materials, Hokkaido University, Sapporo 060-8628, Japan

ARTICLE INFO

Article history:
Received 28 July 2011
Received in revised form 31 October 2011
Accepted 5 November 2011
Available online 11 November 2011

Keywords:
PAN-derived activated carbon
Heat treatment
Nitrogen removal
N_2 formation
Fe catalyst

ABSTRACT

Polyacrylonitrile-derived activated carbon as a model of coal char has been heated in high-purity He at 10 °C/min up to 1000 °C with a flow-type fixed bed quartz reactor, and the catalysis of N_2 formation by precipitated iron has been investigated by use of XPS, TEM and XRD methods. Fine iron particles with the average size of 15 nm increase remarkably the formation rate between 600 and 1000 °C, and N_2 yield up to 1000 °C reaches about 65% at 1.9 mass% Fe. The XPS and XRD measurements after heat treatment exhibit that nitrogen functionality does not change significantly, but carbon crystallization occurs through the dissolution of iron nanoparticles into the carbon substrate. The *in situ* XRD analyses during heating reveal the formation of austenite that is solid solution of Fe and N (and/or C). Interestingly, the catalysis of N_2 formation by iron and the formation of austenite occur at almost the same temperature range of 600–1000 °C. It is thus likely that nanoscale iron particles move in the carbon matrix and react with heterocyclic nitrogen in order to produce the solid solution, which is subsequently decomposed into N_2.

1. Introduction

The nitrogen present in coal (coal-N) exists predominantly in thermally stable heterocyclic structures, such as pyridinic and pyrrolic forms [1,2]. When coal is burned with air in a combustion furnace in order to produce electricity, the pyrolysis first takes place: volatile components such as gas and tar are released, whereas mineral matter and fixed carbon, which is composed mainly of condensed aromatic structures, are retained as char. Subsequently, gas and tar are combusted with O_2 in air, and the carbon is then burned. In the similar way, coal-N is first pyrolyzed and transformed into volatile-N (tar-N, HCN and NH_3) and char-N. Because the partitioning of coal-N to gas, tar and char species in the pyrolysis step is one of the important factors determining NO_x and N_2O emissions in the subsequent combustion process [3–6], the pyrolytic behavior of coal-N has been examined extensively and reviewed by several workers [4,5,7–10]. Since char-N may make the major contribution to the formation of NO_x and N_2O [3,11], efficient nitrogen removal as N_2 from char-N at the pyrolysis stage might lead to significant reduction of these nitrogen oxides.

The present authors' group has been working on the fate of coal-N upon pyrolysis, in particular focusing on the formation of inert N_2 from many coals with different ranks [12–14], though most of the researchers have paid no attention to this topic. We have shown that char-N is the major source of N_2, and that nanoscale particles of metallic iron, which are formed from Fe^{3+} cations added to low rank coals [15,16] or naturally present in them [13,14], can catalyze the transformation of char-N to N_2 at 750–1000 °C. These findings are interesting from the above-mentioned viewpoints. Although it has also been suggested that the iron-catalyzed conversion of char-N to N_2 may occur via solid–solid interactions of iron nanoparticles with pyridinic and pyrrolic forms [16,17], no mechanistic studies have been made in more detail so far. In the present paper, therefore, the main objective is to clarify how iron–nitrogen interactions occur in the carbon matrix of char. For this purpose, polyacrylonitrile-derived activated carbon with heterocyclic nitrogen structures, denoted as PAN carbon, is used as a model of coal char, because it does not contain any metal impurities that may affect the main purpose of this work but includes the nitrogen amount sufficient for the detailed analysis and characterization. We first investigate the influence of nano-ordered iron catalyst on N_2 formation in the temperature-programmed heat treatment of PAN carbon, and then elucidate iron–nitrogen interactions at solid phase by means of XPS, TEM and XRD techniques.

2. Experimental

2.1. Carbon sample

PAN carbon was prepared in the following manner. Commercially available polyacrylonitrile, which was obtained from Polyscience, Inc., was first carbonized in a stream of He at 1000 °C

* Corresponding author. Tel.: +81 11 706 6850; fax: +81 11 726 0731.
E-mail address: tsubon@eng.hokudai.ac.jp (N. Tsubouchi).

0926-3373/$ – see front matter © 2011 Elsevier B.V. All rights reserved.
doi:10.1016/j.apcatb.2011.11.014

for 30 min, and then activated in 20 vol% O_2/He at 500 °C for 100 min. The C, H, N and O contents in PAN carbon with size fraction of 44–74 μm were 79.3, 0.4, 6.8 and 13.5 mass%-dry, respectively. Since it has been reported that coal chars after pyrolysis at 500–900 °C contain C, H, N and O elements in the concentration range of about 75–95, 0.1–3.0, 0.5–2.5 and 2.0–20 mass%-daf, respectively [18], the present carbon sample may be regarded as N-enriched model char. The BET surface area of the PAN carbon analyzed by the N_2 adsorption method was 480 m^2/g, which was about 10 times larger than that (5 m^2/g) without any activation.

2.2. Iron addition

An aqueous solution of $FeCl_3$ was used as a catalyst precursor, because it is readily available as the main component of acid wastes from iron and steel pickling plants. A Cl-free iron catalyst in highly dispersed forms was precipitated onto the PAN carbon from $FeCl_3$ solution by using $Ca(OH)_2$. The procedure has been described in detail earlier [19] and is thus simply explained below. A mixture of the carbon and $FeCl_3$ solution was stirred at room temperature, and a sufficient amount of $Ca(OH)_2$ powder was then added to precipitate the iron as FeOOH onto the carbon surface according to the following equation:

$$2FeCl_3 + 3Ca(OH)_2 \rightarrow 2FeOOH + 3CaCl_2 + 2H_2O \quad (1)$$

The resulting iron-loaded carbon was separated from the solution by filtration, then washed repeatedly with purified water in order to remove excess $Ca(OH)_2$, and finally dried in a flow of N_2 at 110 °C for 60 min. Fe loading was controlled by changing the initial concentration of $FeCl_3$ in water, and the actual loading in the dried sample, determined by the atomic absorption spectroscopy method after acid leaching [19], was 0.9 or 1.9 mass% as the metal. Further, Cl determination of each sample by a standard Eschka method (ISO 587-1981 (E)) exhibited that the iron was free from Cl contamination. The Cl ions in $FeCl_3$ solution could thus be removed completely as water-soluble $CaCl_2$ according to Eq. (1).

The Mössbauer and Fe 2p XPS measurements have revealed that Fe cations, which are precipitated onto the surface of an Australian brown coal by the same method as mentioned above, exist as fine particles of FeOOH [20]. The same Fe 2p XPS spectra were detectable for the present samples with Fe cations precipitated, and atomic Fe/C ratios determined by the XPS were larger than those obtained by the elemental analysis. These observations show that the present iron catalysts are also in the form of fine particles of FeOOH on the carbon surface. The N 1s XPS and elemental analyses exhibited that there was no significant difference between the surface and bulk N/C ratios (7.0×10^{-2} to 7.1×10^{-2}), which were almost unchanged before and after catalyst addition.

2.3. Heat treatment

All experiments were made in a temperature-programmed mode with a fixed bed quartz reactor. The details of the apparatus have been described earlier [12]. In the run, about 180 mg of the PAN carbon or iron-loaded carbon was first charged into a rectangular quartz cell on a quartz holder in the reactor, and special care was then taken in order to ensure that the whole reaction system was free from any leakage. After such prudent precautions, the reactor was heated at 10 °C/min up to 1000 °C in a stream of high-purity He (>99.9999%), soaked for 60 min, and then quenched to room temperature. The flow rate was controlled at 100 cm^3 (STP)/min, which corresponded to a linear velocity of 0.33 mm/s at atmospheric pressure.

2.4. Nitrogen analysis

The N_2 in the effluent from the reactor outlet was determined online at intervals of 5 min with a high-speed micro gas chromatograph (GC) (Microsensor Technology, Inc., M200). The effluent was also collected into an aluminum-laminated plastic bag, and the HCN and NH_3 in the bag were measured with a Fourier transform infrared spectrometer (FT-IR) (Bio-Rad, Inc., FTS40A) equipped with a long-path gas cell. The carbonaceous residue remaining in the cell after heat treatment was recovered as char, and the N in the char (char-N) was determined with a conventional nitrogen analyzer (Yanaco Analytical Instruments Corp., MT500HC/MTS1). Any tarry materials were not observed under the present conditions. In addition, no NO and N_2O were also detectable by the FT-IR method. These observations may be reasonable, because no significant amounts of volatile matters are released during heat treatment of PAN carbon samples. Yield of N_2, HCN, NH_3 or char-N was expressed in percent of total nitrogen in feed sample. Nitrogen mass balances for all runs fell within the reasonable range of 94–106%, which indicates that all of the analytical methods used for N determination are reliable.

2.5. XPS analyses and TEM observations

The X-ray photoelectron spectroscopy (XPS) measurements were carried out with a non-monochromatic Mg-Kα source operating at 240 W (Shimadzu Corp., ESCA750) in order to examine the chemical forms of the N and Fe on the surfaces of iron-bearing chars. The specimens were made into fine powders just before each XPS analysis and mounted onto a sample holder using Ag paste. Long acquisition times of several hours were used in order to obtain good resolution for the N 1s and Fe $2p_{3/2}$ spectra, and their binding energies were referred to the Ag $3d_{5/2}$ peak at 367.9 eV. Least-squares curve-fitting analyses of N 1s spectra were made using Gaussian peak shapes. Upon deconvolution, the binding energy of each peak and the full width at half-maximum (fwhm) value were fixed within ±0.1 eV, and only the amplitude was varied in order to obtain the optimum curve resolution [17].

Char samples after heat treatment at 600–1000 °C were further characterized with a high resolution transmission electron microscope (TEM) (JEOL, Ltd., JEM3010) at a resolution of 0.2 nm and at an accelerating voltage of 300 kV. The average size and size distribution of iron particles were estimated by counting 100 particles from representative TEM images of each sample. The analytical conditions have been described in detail previously [17].

2.6. XRD measurements

The powder X-ray diffraction (XRD) analyses of iron-bearing chars cooled to room temperature after heat treatment were conducted with an X-ray diffractometer (Shimadzu Corp., XRD6000) using Mn-filtered Fe-Kα radiation (30 kV, 40 mA) in order to identify crystalline forms of iron catalysts and evaluate carbon structures quantitatively. Changes in iron forms during heating were also examined by the *in situ* XRD technique, in which about 50 mg of the PAN carbon with 1.9 mass% Fe was heated up to 655–1025 °C under the same conditions as in the temperature-programmed heat treatment mentioned above. The C (0 0 2) signal after removal of the diffraction background was deconvoluted into amorphous (A-) (31.1°) and turbostratic (T-) (33.1°) carbon by the curve-fitting method using Gaussian peak shapes [21–23]. The reproducibility of the present deconvolution analysis fell within ±3% in every case.

3. Results and discussion

3.1. N_2 formation and nitrogen distribution

The rate profiles of N_2 formation in the temperature-programmed heat treatment of PAN carbon samples without and with the precipitated iron are shown in Fig. 1, where the abscissa has the 2 functions of temperature and soaking time at 1000 °C. In the absence of the catalyst, N_2 started to evolve after 500 °C, and the rate increased gradually with increasing temperature, but it decreased during holding the sample at 1000 °C. When 0.9 mass% Fe was added to the carbon, the catalytic effect on N_2 formation appeared apparently around 600 °C, which was much lower than the temperature (750 °C) observed during fluidized bed pyrolysis at 600–700 °C/min of low rank coals with precipitated iron [10,15–17]. Such a difference would be ascribed to slower heating rate in the present work than in the fluidized bed pyrolysis. As shown in Fig. 1, the Fe promoted N_2 formation predominantly at the temperature range of 600–1000 °C, and the rate enhancement by Fe addition became highest at 800 °C. When Fe loading (Fe%) was raised to 1.9 mass%, the rate around 700–900 °C tended to increase further, and the maximal rate observed at 800 °C was approximately 10 times that without the catalyst (Fig. 1).

Fig. 2 presents nitrogen distribution after 60 min soaking at 1000 °C. N_2 yield was calculated by integrating each profile shown in Fig. 1. With PAN carbon without any Fe added, N_2 was the predominant N-containing gas followed by HCN, and yields of both

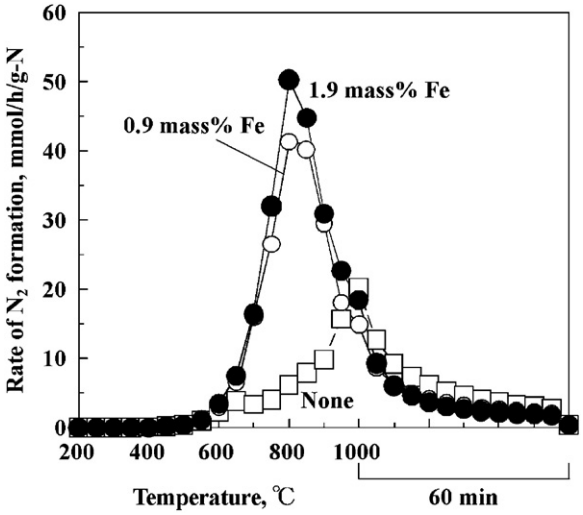

Fig. 1. Rate profiles for N_2 formation in the temperature-programmed heat treatment of PAN carbon samples without and with 0.9 or 1.9 mass% Fe.

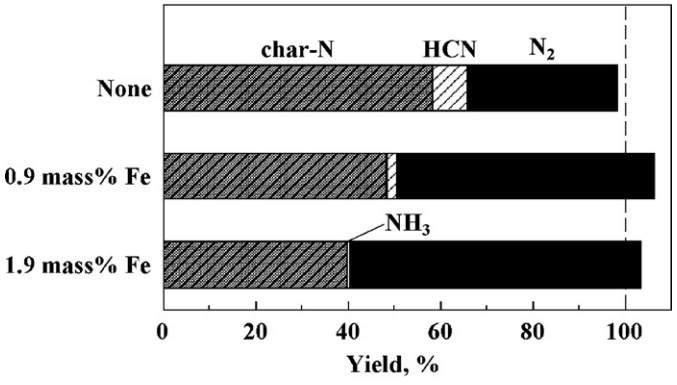

Fig. 2. Nitrogen distribution after heat treatment at 1000 °C.

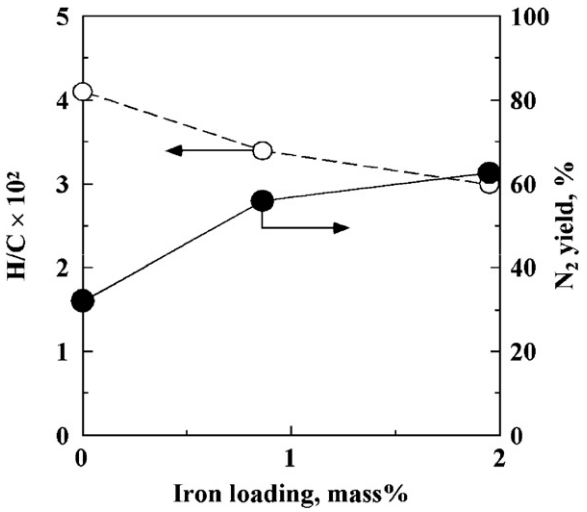

Fig. 3. Influence of iron loading on atomic H/C ratio in char and N_2 yield.

species were 32 and 9%, respectively. No NH_3 was detected under the conditions applied. According to previous work [24], it has been widely accepted that the formation of N_2 and HCN from PAN-derived carbons occurs via condensation reactions of the ladder polymers including heterocyclic nitrogen, such as pyridinic and pyrrolic forms. As provided in Fig. 2, the addition of 0.9 mass% Fe to the PAN carbon increased N_2 yield considerably but decreased HCN and char-N. Since it has been reported that Fe^{3+} ions inherently present in low rank coals and externally added to them can catalyze secondary decomposition reactions of tar-N, HCN and NH_3 into N_2 during pyrolysis process [10,12–17], it is probable that the HCN decreased by Fe addition is converted to N_2. When Fe% was increased to 1.9 mass%, the increase in N_2 and the decrease in char-N took place mainly, and the former yield reached approximately 65%, which was about 2 times higher than that without the catalyst (Fig. 2). These results point out that the iron catalyst can promote N_2 formation from not only HCN but also char-N.

The Fe% dependence of atomic H/C ratio in each 1000 °C-char is shown in Fig. 3, where N_2 yields in Fig. 2 are also given for comparison. The ratio tended to be smaller at a higher Fe% and exhibited the reverse dependence on Fe%, compared with the case of N_2. Because the decrease in H/C ratio by Fe addition means the occurrence of aromatization reactions, the conversion of heterocyclic nitrogen forms to N_2 in the presence of the iron catalyst may occur in the process of carbon crystallization. This point will be discussed in detail later.

3.2. Functional forms of nitrogen and iron at surface

Fig. 4 illustrates the N 1s XPS spectra of PAN carbon samples with 1.9 mass% Fe before and after heat treatment. The XPS intensity observed was lower with the char after heat treatment at a higher temperature, whereas the spectrum shape was broad in the binding energy range of 395–405 eV with all the samples. As seen in broken lines in Fig. 4, the least-squares curve-fitting analysis exhibited that four major Gaussian components existed at 398.6, 400.3, 401.5 and 403.0 eV. The former three components corresponded to pyridinic-N, pyrrolic-N and quaternary-N, respectively [1,7,17,18]. The latter one may be identified to oxidized-N [1], which might be formed during O_2-activation of PAN sample after carbonization and/or upon exposure to laboratory air for char recovery from the reactor [25]. All the nitrogen functional forms mentioned above can also be observed in coal and char [1,7,17,18].

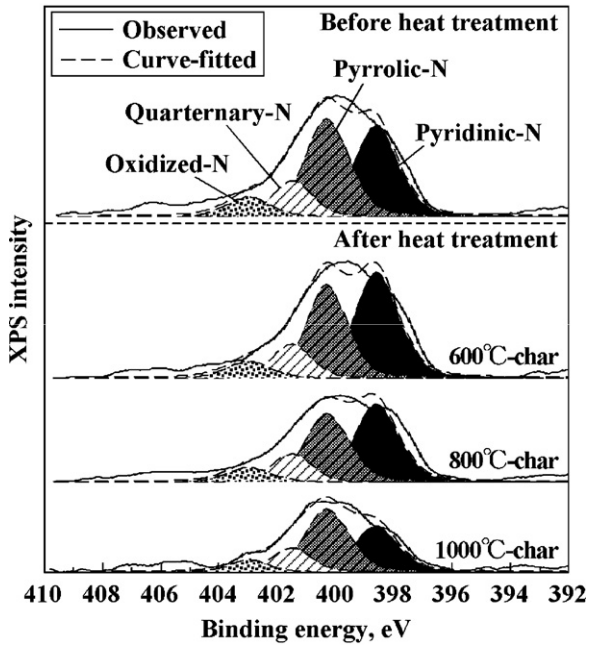

Fig. 4. N 1s XPS spectra for PAN carbon samples with 1.9 mass% Fe before and after heat treatment.

As shown in Fig. 4, pyrrolic-N and pyridinic-N were the main N-forms in the Fe-loaded carbon before heat treatment, and quaternary-N succeeded them, oxidized-N being minor. The ratio of pyrrolic-N to pyridinic-N was estimated to be approximately 1.1, which was much smaller than those (1.6–1.8) observed for coal chars after pyrolysis at 750–900 °C with a Pyroprobe [26] and a fluidized bed reactor [17]. When this sample was heated up to 600–1000 °C, the distribution of the four N-groups was significantly unchanged (Fig. 4). This observation suggests that N_2 evolves from these groups at almost the same rate. According to our study [17], the iron precipitated onto an Australian brown coal is effective for preferential formation of N_2 from pyrrolic-N. The difference may be related with a larger ratio (1.6) of pyrrolic-N/pyridinic-N in the latter case.

Fig. 5 presents the Fe $2p_{3/2}$ XPS spectra of the 800 °C-char shown in Fig. 4. The char without Ar sputtering exhibited the broad profile in the binding energy range of 708–714 eV. Since it has been well-accepted that the Fe $2p_{3/2}$ peaks of magnetite (Fe_3O_4), wustite ($Fe_{1-x}O$) and hematite (α-Fe_2O_3) appear at 708.1–711.5, 709.3–710.5 and 710.2–711.6 eV, respectively [27,28], such oxides are likely to be the major Fe-forms on the char surface. The oxides

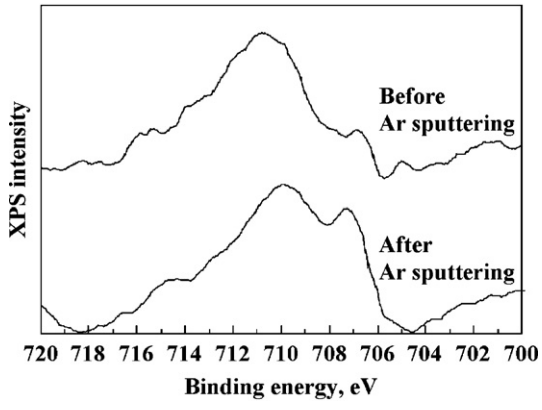

Fig. 5. Fe $2p_{3/2}$ XPS spectra before and after Ar sputtering for the same 800 °C-char as in Fig. 4.

must be formed by oxidation of metallic iron (α-Fe) upon exposure to laboratory air for char recovery, because the powder XRD and *in situ* XRD experiments revealed the presence of α-Fe as the bulk species as mentioned later (Figs. 8 and 9). When this sample was etched by Ar ion bombardment for 30 min, surface iron oxides at 711–714 eV were removed, and the $2p_{3/2}$ peak of α-Fe appeared clearly at 707 eV [27,28] (Fig. 5). Such a trend was also observed with all char samples shown in Fig. 4. These results mean the transformation of the iron precipitated as fine particles of FeOOH onto PAN carbon to α-Fe upon heat treatment.

3.3. Size of iron particles

Fig. 6 illustrates the TEM micrographs of char samples after heat treatment of PAN carbon with 1.9 mass% Fe. The average size of iron particles at 600 °C, that is, before the start of the iron-catalyzed N_2 formation (Fig. 1), was as fine as 15 nm (Fig. 6a). It has been reported that $Fe(NO_3)_3$ impregnated with an activated carbon microfiber from phenol resin is transformed into fine particles of metallic iron with the average crystalline size of approximately 15 nm during H_2 reduction at 600 °C [29,30]. As seen in Fig. 6b and c, the average particle sizes at 800–1000 °C, 25–30 nm, were larger than that at 600 °C, showing the agglomeration of iron particles via their migration within the char matrix. When the Fe was precipitated onto PAN-derived carbon without O_2-activation in the same manner as mentioned above, the average size at 1000 °C was as large as 70 nm, and the iron was almost inactive catalytically for N_2 formation [31]. According to earlier work on the development of active iron catalysts for coal gasification at low temperatures [19], it has been accepted that Fe^{3+} ions in the precipitation process using $FeCl_3$ solution interact strongly with free O-functional groups unassociated with metal ions naturally present in coal, which means the high degree of iron dispersion in the catalyst precipitation step. Because the activation of PAN-derived carbon increased not only the surface area but also the amount of O-functional groups [31], the formation of smaller nanoparticles on the chars provided in Fig. 6 is possibly attributed to higher dispersion of the precipitated iron.

Fig. 7 illustrates the particle size distribution of iron catalysts in the same samples as in Fig. 6. Most of iron particles in the 600 °C-char were below 20 nm in size (Fig. 7a), whereas more than half of them were above 20 nm at 800–1000 °C, and the iron with the size of 40–60 nm was also observed (Fig. 7b and c). When Fe loading was decreased from the usual 1.9 to 0.9 mass%, the iron with the size of $\geq$35 nm could not be detected apparently, and the average particle size at 1000 °C was as fine as 15 nm. These observations indicate a larger degree of catalyst agglomeration at a higher loading.

Fig. 6b and c also revealed that lamella structures attributable to graphitized carbon existed clearly in the vicinity of iron particles in the 800 °C- and 1000 °C-chars, respectively, but they were not so developed. These results suggest the formation of T-carbon, which can be regarded as crystallized (partly graphitized) carbon [21,22]. As shown in Fig. 6a, lamella structures were not observed in the 600 °C-char. Further, the formation of larger iron particles at higher temperatures above 800 °C (Figs. 6 and 7) is likely to mean that smaller nanoparticles readily migrate in the char substrate and consequently agglomerate. It is thus possible that carbon crystallization takes place significantly in the migration process.

3.4. Crystalline forms of iron catalysts and quantitative elucidation of carbon structures

Any Fe-species were not detectable by XRD measurement of PAN carbon with 0.9 or 1.9 mass% Fe before heat treatment. These observations indicate the presence of the highly dispersed iron on the carbon. It has been shown by the Mössbauer and XPS analyses

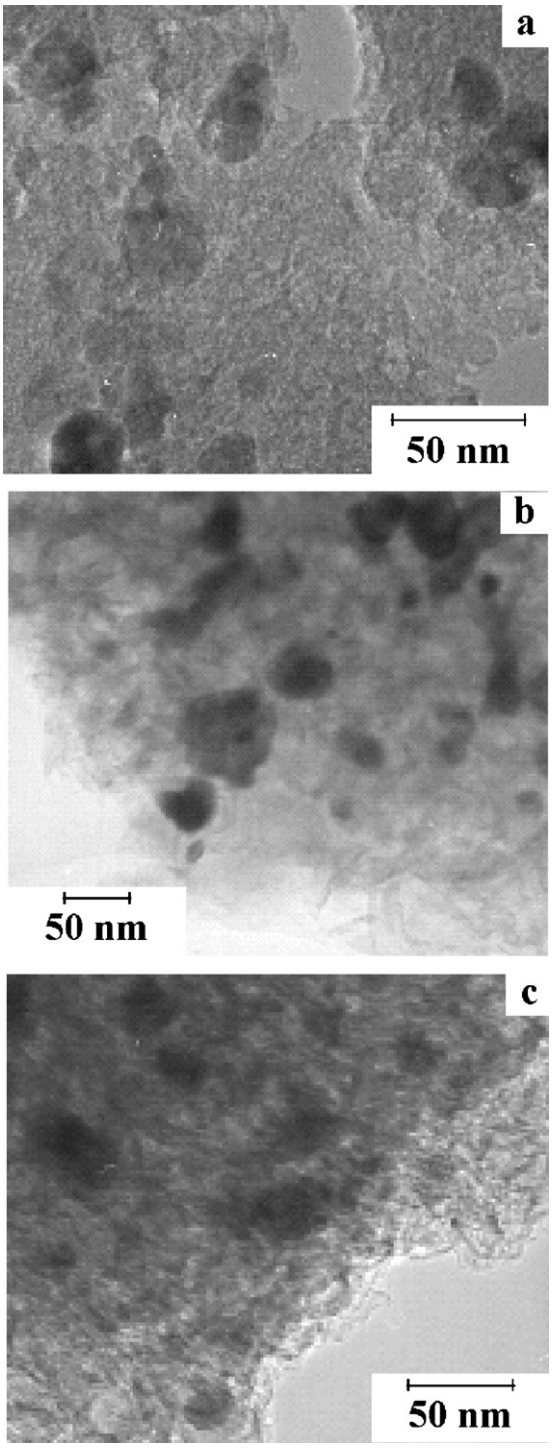

Fig. 6. TEM micrographs of the chars after heat treatment at 600 °C (a), 800 °C (b) and 1000 °C (c) of PAN carbon with 1.9 mass% Fe.

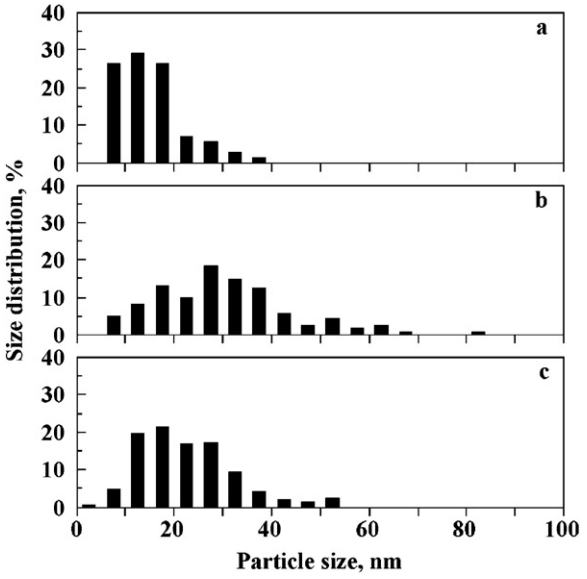

Fig. 7. Particle size distribution for iron catalysts in the same chars as in Fig. 6: (a) 600 °C, (b) 800 °C and (c) 1000 °C.

that iron catalyst precipitated onto brown coal by the same method as in this work is present in the form of fine particles of FeOOH [20].

Fig. 8 shows the XRD profiles of char samples cooled to room temperature after heat treatment. When PAN carbon with 1.9 mass% Fe was heated up to 600 °C, the weak diffraction signals of Fe_3O_4 and $Fe_{1-x}O$ were observed, which means the transformation of the initial FeOOH to these oxide forms. At 800–1000 °C, the oxide species disappeared almost completely, and instead the XRD peaks of α-Fe and cementite (Fe_3C) appeared. These observations show not only almost complete reduction of Fe_3O_4 and $Fe_{1-x}O$ to α-Fe but also the reaction of α-Fe with the carbon substrate between 600 and 1000 °C. In addition, the XRD results suggest that the oxide species or both α-Fe and Fe_3C may be included in the iron particles detected by the TEM observations (Fig. 6) of the 600 °C-char or the 800–1000 °C-chars, respectively.

Fig. 8 also provides information about carbon structures due to C (0 0 2) diffraction lines. When the XRD profiles after heat treatment of the carbon samples with and without the Fe were compared, the C (0 0 2) peaks were stronger and sharper in the Fe-bearing chars. In other words, the diffraction lines of T-carbon at 2θ (Fe-Kα) of 33.1° appeared more distinctly in the presence of the Fe. In order to evaluate this point quantitatively, all the C (0 0 2) signals observed were deconvoluted into A- and T-carbon (broken lines in Fig. 8). The results are given in Table 1. The proportion of T-carbon in char samples without any Fe added was as low as 1–2%. In the presence of 0.9 or 1.9 mass% Fe, on the other hand, the value increased with increasing temperature to be approximately 20%

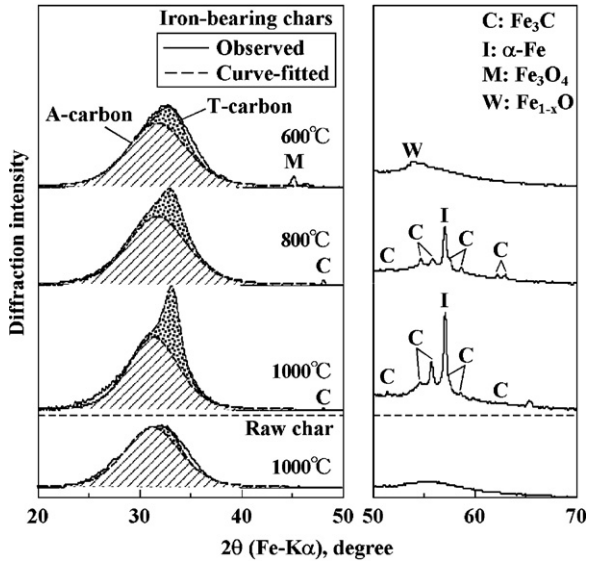

]

Fig. 8. XRD profiles for some chars cooled to ambient temperature after heat treatment of PAN carbon samples with and without 1.9 mass% Fe.

Table 1
Carbon structures of chars after heat treatment.

Iron loading (mass%-dry)	Temperature (°C)	Type of carbon	
		A-carbon[a] (%)	T-carbon[b] (%)
0	600	99	1
0	1000	98	2
0.9	600	87	13
0.9	1000	82	18
1.9	600	86	14
1.9	800	84	16
1.9	1000	80	20

[a] Proportion of amorphous carbon in char.
[b] Proportion of turbostratic carbon in char.

at 1000 °C. The formation of Fe_3C (Fig. 8) and T-carbon indicates that the iron first dissolves in the char substrate and subsequently catalyzes crystallization reactions of A-carbon [21,22]. It can readily be expected that the iron reacts with heterocyclic nitrogen forms in the char matrix in the process of carbon crystallization.

Fig. 9 illustrates the *in situ* XRD profiles during heating the carbon with 1.9 mass% Fe. At 655 °C, α-Fe was the main crystalline form, and the small peaks attributable to $Fe_{1-x}O$ were also observed. Interestingly, the XRD signals of austenite, solid solution of γ-Fe and N (and/or C), were present as well (Fig. 9a). When the temperature was raised to 815–1025 °C, the XRD intensities of this species increased with a corresponding decrease in the intensity of α-Fe, and austenite became the dominant form in this temperature region (Fig. 9b–d). When the sample heated up to 1025 °C was quenched to room temperature, α-Fe, Fe_3C and T-carbon were formed (Fig. 9e), in harmony with the XRD profile for the Fe-bearing 1000 °C-char in Fig. 8.

3.5. Possible mechanisms for iron-catalyzed formation of N_2

The main objective of this section is to elucidate the mechanism of the iron-catalyzed conversion of heterocyclic nitrogen forms (Fig. 4) to N_2 (Fig. 1). As described above, fine particles of FeOOH precipitated onto PAN carbon were first transformed into

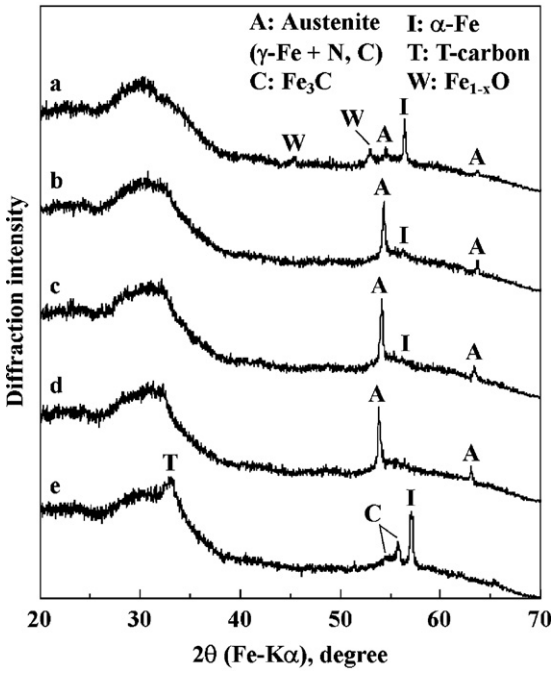

Fig. 9. *In situ* XRD profiles during heat treatment of PAN carbon with 1.9 mass% Fe: (a) 655 °C, (b) 815 °C, (c) 920 °C, (d) 1025 °C and (e) cooling to room temperature after heating up to 1025 °C.

Fe_3O_4 and $Fe_{1-x}O$ during heat treatment (Fig. 8), and most of these oxide forms were then reduced to α-Fe nanoparticles up to 650 °C (Figs. 6, 7 and 9). These results indicate the evolution of sufficient reducing gases (for example, CO and H_2) for catalyst reduction. In order to confirm this point, the concentrations of CO and H_2 in the reactor exit during heat treatment of PAN carbon samples were mainly measured with the GC, and the results obtained showed that the presence of 0.9 or 1.9 mass% Fe lowered total amount of CO evolved up to 650 °C and simultaneously increased that of CO_2. Since no significant amount of H_2 was produced below 650 °C, irrespective of the absence or presence of the catalyst, the reduction of the precipitated iron may mainly be caused by CO formed from the carbon. According to thermodynamic calculations, the standard Gibbs free energy changes (ΔG) for the reactions (Eqs. (2)–(4)) of CO with FeOOH, Fe_3O_4 and FeO at 300–650 °C are −7 to −14, −2 to +1 and −1 to 0 kcal/mol, respectively.

$$FeOOH + 0.25CO \rightarrow 0.25Fe_3O_4 + 0.25FeO + 0.5H_2O + 0.25CO_2 \quad (2)$$

$$Fe_3O_4 + 4CO \rightarrow 3Fe + 4CO_2 \quad (3)$$

$$FeO + CO \rightarrow Fe + CO_2 \quad (4)$$

It is thus possible that α-Fe is mainly formed via Eqs. (2)–(4) below 650 °C and too fine (<5 nm) to be detected by XRD. The combination of Eqs. (2)–(4) can lead to the following overall equation for the formation of metallic iron.

$$FeOOH + 1.5CO \rightarrow Fe + 1.5CO_2 + 0.5H_2O \quad (5)$$

It should be noted that the catalysis of N_2 formation by iron (Fig. 1) and the formation of austenite (Fig. 9) take place at almost the same temperature range of 600–1000 °C. On the basis of the phase diagrams of the Fe–N and Fe–C systems [32], it has been widely accepted that the solid solubility limit of nitrogen into metallic iron increases significantly from 0.4 to 9.0 at.% at about 590 °C where α-Fe is transformed into γ-Fe, whereas carbon can dissolve rapidly into γ-Fe at 740 °C. Thus, the former temperature corresponded well to the onset of the iron-catalyzed formation of N_2 (Fig. 1). It is likely that the austenite formed below 740 °C is the solid solution of γ-Fe and N, and that N_2 formation in this temperature range proceeds through the intermediate. The austenite may be converted to iron nitrides (for example, Fe_xN), which may subsequently decompose in order to provide N_2 [10,16,17]. It has been reported that Fe_2N and Fe_4N are thermally unstable at ≥480 and 680 °C, respectively [32].

The austenite formed above 740 °C may be composed of γ-Fe, N and C, and transformed into Fe_xN_yC as well as Fe_xN. The formation of Fe_xN_yC and the subsequent decomposition into N_2 may involve carbon crystallization, that is, the transformation of A-carbon to T-carbon (Figs. 8, 9 and Table 1). Because it has been accepted that the catalysis of carbon crystallization by transition metals occurs through carbon dissolution into metal particles followed by the decomposition of metal carbides [21,22], the following mechanism can be proposed for the formation of T-carbon in the presence of the precipitated iron.

$$\gamma\text{-Fe} + \text{A-carbon} \rightarrow Fe_3C \quad (6)$$

$$Fe_3C \rightarrow \gamma\text{-Fe} + \text{T-carbon} \quad (7)$$

As seen in Figs. 8 and 9, Fe_3C was actually detected in the Fe-bearing chars after heat treatment at 800–1025 °C. In the process of carbon crystallization, γ-Fe particles may also react with heterocyclic nitrogen, such as pyrrolic-N and pyridinic-N (Fig. 4), in order to produce Fe_xN_yC, which may subsequently undergo decomposition reactions into N_2. The XPS analyses after pyrolysis of

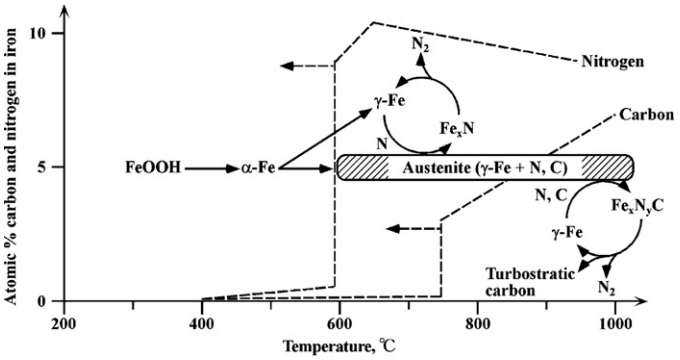

Fig. 10. Proposed routes for iron-catalyzed formation of N_2 at solid phase.

iron-exchanged brown coal at 900 °C suggested strong interactions between iron particles and char-N [17].

On the basis of the above-described results and discussion, several routes for the iron-catalyzed formation of N_2 at solid phase are roughly drawn in Fig. 10. The formation of T-carbon provided in Figs. 8 and 9 might prevent iron particles from moving within the char matrix. As seen in Figs. 6 and 7, the TEM observations showed that catalyst agglomeration occurred in the process of N_2 formation. The lowering in both mobility and activity of iron particles may be responsible for the decreased rate of N_2 formation observed after 800 °C (Fig. 1).

4. Conclusions

In order to make clear the influence of iron catalyst on N_2 formation during coal pyrolysis, fine particles of FeOOH are precipitated onto polyacrylonitrile-derived activated carbon as a model of coal char, and the resulting sample is heated in an inert gas at 10 °C/min up to 1000 °C with a fixed bed quartz reactor. Fine iron particles with the average size of 15 nm promote N_2 formation remarkably at the temperature range of 600–1000 °C, and the catalytic effect is largest at 800 °C. Catalyst agglomeration occurs in the heat treatment process. The N 1s XPS analyses exhibit that pyrrolic-N and pyridinic-N are the main N-forms in the original sample, and such nitrogen functionality is significantly unchanged upon heat treatment. The XRD measurements show that iron nanoparticles can also promote transformation reactions of amorphous carbon to turbostratic carbon, meaning the dissolution of the iron into the carbon substrate. Further, the *in situ* XRD analyses during heating reveal the formation of solid solution of Fe and N (and/or C). On the basis of the above results, it is likely that the iron-catalyzed conversion of heterocyclic nitrogen to N_2 proceeds through formation of the solid solution and subsequent decomposition into N_2.

Acknowledgment

The present work was supported in part by the Proposal-Based New Industry Creative Type Technical R&D Promotion Program from the New Energy and Industrial Technology Development Organization (NEDO), Japan.

References

[1] S.R. Kelemen, M.L. Gorbaty, P.J. Kwiatek, Energy Fuels 8 (1994) 896–906.
[2] O.C. Mullins, S. Mitra-Kirtley, J. van Elp, S.P. Cramer, Appl. Spectrosc. 47 (1993) 1268–1275.
[3] K.M. Thomas, Fuel 76 (1997) 457–473.
[4] M.A. Wójtowicz, J.R. Pels, J.A. Moulijn, Fuel Process. Technol. 34 (1993) 1–71.
[5] J.E. Johnsson, Fuel 73 (1994) 1398–1415.
[6] P. Glarborg, A.D. Jensen, J.E. Johnsson, Prog. Energy Combust. Sci. 29 (2003) 89–113.
[7] R.M. Davidson, Nitrogen in Coal, IEA Coal Research, London, 1994, IEAPER/08.
[8] J. Leppälahti, T. Koljonen, Fuel Process. Technol. 43 (1995) 1–45.
[9] C-Z. Li, Advances in the Science of Victorian Brown Coal; Conversion of Coal-N and Coal-S during Pyrolysis, Gasification and Combustion, Elsevier, Amsterdam, 2004 (chapter 6).
[10] N. Tsubouchi, Y. Ohtsuka, Fuel Process. Technol. 89 (2008) 379–390.
[11] K. Makino, J. Jpn. Inst. Energy 72 (1993) 401–402.
[12] Z. Wu, Y. Ohtsuka, Energy Fuels 11 (1997) 477–482.
[13] Z. Wu, Y. Ohtsuka, Energy Fuels 11 (1997) 902–908.
[14] Y. Ohtsuka, Z. Wu, Energy Fuels 23 (2009) 4774–4781.
[15] Y. Ohtsuka, H. Mori, T. Watanabe, K. Asami, Fuel 73 (1994) 1093–1097.
[16] H. Mori, K. Asami, Y. Ohtsuka, Energy Fuels 10 (1996) 1022–1027.
[17] Y. Ohtsuka, T. Watanabe, K. Asami, H. Mori, Energy Fuels 12 (1998) 1356–1362.
[18] M.A. Wójtowicz, J.R. Pels, J.A. Moulijn, Fuel 74 (1995) 507–516.
[19] K. Asami, Y. Ohtsuka, Ind. Eng. Chem. Res. 32 (1993) 1631–1636.
[20] Y. Ohtsuka, K. Asami, Catal. Today 39 (1997) 111–125.
[21] A. Ōya, S. Ōtani, Carbon 19 (1981) 391–400.
[22] A. Ōya, H. Marsh, J. Mater. Sci. 17 (1982) 309–322.
[23] N. Tsubouchi, C. Xu, Y. Ohtsuka, Energy Fuels 17 (2003) 1119–1125.
[24] E. Fitzer, W. Frohs, M. Heine, Carbon 24 (1986) 387–395.
[25] J.R. Pels, F. Kapteijn, J.A. Moulijn, Q. Zhu, K.M. Thomas, Carbon 33 (1995) 1641–1653.
[26] S. Kambara, T. Takarada, Y. Yamamoto, K. Kato, Energy Fuels 7 (1993) 1013–1020.
[27] J.F. Moulder, W.F. Stichle, P.E. Sobol, K.D. Bomben, in: J. Chastain (Ed.), Handbook of X-ray Photoelectron Spectroscopy, Perkin-Elmer, Eden Prairie, 1992.
[28] C.D. Wagner, A.V. Naumkin, A. Kraut-Vass, J.W. Allison, C.J. Powell, J.R. Rumble Jr., NIST X-ray Photoelectron Spectroscopy Database; NIST Standard Reference Database 20, version 3.5 (Web version), NIST, Gaithersburg, 2007.
[29] A.K. Gupta, D. Deva, A. Sharma, N. Verma, Ind. Eng. Chem. Res. 49 (2010) 7074–7084.
[30] H. Katepalli, M. Bikshapathi, C.S. Sharma, N. Verma, A. Sharma, Chem. Eng. J. 171 (2011) 1194–1200.
[31] Y. Ohshima, Y. Wang, N. Tsubouchi, Y. Ohtsuka, Am. Chem. Soc. Div. Fuel Chem. Prepr. 45 (2000) 335–338.
[32] T.B. Massalski, Binary Alloy Phase Diagrams, 2nd ed., ASM International, Ohio, 1990.